RESEARCH ARTICLE

Key Points:
- This is the first detection of a Southern Hemisphere planetary radar system
- Future Southern Hemisphere radar observations will augment existing Northern Hemisphere capabilities

Correspondence to:
C. Benson,
c.benson@adfa.edu.au

First Detection of Two Near-Earth Asteroids With a Southern Hemisphere Planetary Radar System

Craig Benson[1] ID, John Reynolds[2], N. J. S. Stacy[3], Lance A. M. Benner[4], P. G. Edwards[2], Graham Baines[5], Russell Boyce[1], Jon D. Giorgini[4], Joseph S. Jao[4], George Martinez[4], Martin A. Slade[4] ID, Lawrence P. Teitelbaum[4] ID, Aseel Anabtawi[4], Daniel Kahan[4], Kamal Oudrhiri[4], C. J. Philips[2], J. B. Stevens[2], Ed Kruzins[5] ID, and T. Joseph W. Lazio[4]

[1]School of Engineering and Information Technology, University of New South Wales, Canberra, ACT, Australia, [2]CSIRO Astronomy and Space Science, Australia Telescope National Facility, CSIRO, Epping, New South Wales, Australia, [3]Defence Science and Technology Group, Adelaide, South Australia, Australia, [4]Jet Propulsion Laboratory, California Institute of Technology, Pasadena, CA, USA, [5]CSIRO Astronomy and Space Science, Canberra Deep Space Communications Complex, Tuggeranong, ACT, Australia

Abstract We describe the first demonstration of a Southern Hemisphere planetary radar system to detect two near-Earth asteroids (NEAs). The demonstration was conducted in a bistatic manner, with the 70 m antenna of the Canberra Deep Space Communications Complex transmitting at 2.1 GHz and reception at the Parkes Radio Telescope, outfitted with multiple receivers, and the Australia Telescope Compact Array. This initial system was used to detect the NEAs (43577) 2005 UL5 and (33342) 1998 WT24 during their close approaches in 2015 November and 2015 December, respectively. We describe the performance of the system and consider future possibilities using other antennas of the Canberra Deep Space Communications Complex as transmitters.

Plain Language Summary Planetary radar uses large radio dishes to transmit and receive radar signals off distant objects in the solar system. Careful processing of these signals over periods of several hours allows researchers to very accurately determine orbits, measure rotation rates, and in some cases to map surface features. In the past all of these activities have been performed with assets in the Northern Hemisphere. This paper details the first use of a Southern Hemisphere network for this task. The 70 m dish at the NASA/JPL/CSIRO complex at Tidbinbilla in Canberra, Australia, was used as the transmitter, and the Parkes and Narrabri radio telescopes were used as receivers to successfully detect and track asteroids. A Southern Hemisphere network allows asteroids approaching from the south to be observed, filling in a blind spot in our existing capabilities.

1. Introduction

Radar observations have been used to probe the surfaces of all of the planets with solid surfaces and many smaller bodies in the solar system (Ostro, 2007). Notable findings include characterizing the distribution of water at the south pole of the Moon (Campbell et al., 2003; Stacy et al., 1997), the first indications of water ice in the permanently shadowed regions at the poles of Mercury (Harmon et al., 1994; Slade et al., 1992), polar ice and anomalous surface features on Mars (Muhleman et al., 1991), establishing the icy nature of the Jovian satellites (Ostro & Pettengill, 1978), and the initial characterizations of Titan's surface (Muhleman et al., 1990).

More recently, there has been considerable interest in using radar observations both to characterize near-Earth asteroids (NEAs) and determine their orbits precisely. The motivation for radar observations of asteroids is threefold. First, asteroids represent primitive remnants of the early solar system and characterization of their properties can provide insights into their evolution and parent population(s); second, precise knowledge of their orbits is essential to assess the extent to which they might represent impact hazards to the Earth (Committee to Review Near-Earth-Object Surveys, 2010); and, third, they represent targets for exploration by spacecraft (e.g., Chesley et al., 2014), both robotic and crewed.

Ostro and Giorgini (2004), Giorgini et al. (2008), Giorgini, Slade, et al. (2009), Giorgini, Benner, et al. (2009), and Naidu et al. (2016) have presented analyses of the performance of the current planetary radars (Arecibo

and the Goldstone Solar System Radar (GSSR)). Among their conclusions are that the current planetary radars can reduce orbit uncertainties by as much as a factor of 10^5, with the potential benefit of extending the duration over which impact hazard assessment can be made by a factor of 5. Giorgini et al. (2008), Giorgini, Slade, et al. (2009), and Giorgini, Benner, et al. (2009) noted that a Southern Hemisphere radar capability could double the number of objects capable of being detected by virtue of having additional observing time, while Naidu et al. (2016) conducted an analysis based upon the performance of the antennas used in this demonstration and found a potential increase of 50% for the number of asteroids that could have been observed in 2015. Further, being able to track an asteroid from the Northern Hemisphere into the Southern Hemisphere (or vice versa) would improve the physical characterization, for example, by improving estimates of an asteroid's pole directions due to increased sky motion during radar observations relative to what can be done solely from the Northern Hemisphere. (In order to take full advantage of this benefit, the typical signal-to-noise ratio has to be greater than about 20.) There is also a secondary benefit in that the peak signal-to-noise ratios can occur in the Southern Hemisphere, with a recent example being the close approach of (5604) 1992 FE. While Northern Hemisphere observations are often possible, the signal-to-noise ratios can be factors of several lower. Finally, based on a series of simulations, Giorgini et al.(2008), Giorgini, Slade, et al. (2009), and Giorgini, Benner, et al. (2009) conclude that there is a small, but nonzero, fraction of the potentially impacting population for which their orbits do not allow radar observations from the Northern Hemisphere; notably, Naidu et al. (2016) identified 2015 BP509 as a specific example of an asteroid that was not observable by any Northern Hemisphere radar-capable telescope during its Earth close approach in 2015. While not classified as potentially hazardous, it illustrates the potential value of a Southern Hemisphere system.

As a first demonstration of a Southern Hemisphere radar capability, we identified two NEAs likely to produce sufficiently strong radar echoes to warrant a demonstration for a Southern Hemisphere capability. The first target was the asteroid 2005 UL5, which was discovered by the LINEAR survey and has an estimated diameter of 300 m based on its brightness and assumed albedo. Analysis of light curves indicate that this object is a nonprincipal axis rotator with fundamental periods of 3.5 h and 5.1 h (P. Pravec, private communication, 2015), though it is not clear if it is a short-axis mode or a long-axis mode rotator. It has an *Sq* classification, and its closest approach was on 20 November 2015, when it came within 0.0153 AU (= 5 lunar distances). Based on its orbit, it is classified as a potentially hazardous asteroid (PHA).

The second asteroid, 1998 WT24, had a closest approach to the Earth on 11 December 2015, when it came within 0.028 AU (= 10.9 lunar distances). It is an E-class asteroid, and previous observations showed a polarization ratio characteristic of a rough surface (Busch et al., 2008). It was a particularly compelling target for this demonstration, as it approached from the south and represents an example of how a Southern Hemisphere planetary radar capability would enable the earlier detection of asteroids.

The asteroid 1998 WT24 was studied extensively during an even closer flyby in 2001 December (Busch et al., 2008), when it represented the highest signal-to-noise ratio radar target ever detected. The rotation period (3.7 h) and a detailed shape model were obtained, with notable features of the radar observations showing a rounded shape with two large concavities on one hemisphere, with an effective diameter of 415 m, and a rough surface including possible evidence for a boulder in delay-Doppler radar images. At that time, 1998 WT24 was also the target of two bistatic radar demonstrations in Europe, one involving the GSSR and Medicina and one involving Evpatoria and Medicina (Di Martino et al., 2004).

The plan of this paper is the following. In section 2, we describe the antennas used in the demonstrations and the plan of the observations; in section 3, we present the results of our efforts to detect these two asteroids; and in section 4, we present our conclusions and projections for future Southern Hemisphere radar observations.

2. Observations

We employed a bistatic approach, using the transmitter of Deep Space Station 43 (DSS-43), the 70 m antenna at the Canberra Deep Space Communications Complex, with reception at both the Parkes Radio Telescope and the Australia Telescope Compact Array (ATCA).

Table 1 summarizes the observations, which were conducted over the course of several days in 2015 November and December. While all of the antennas are well known, their use in this fashion is novel, and, for completeness, we describe their characteristics as they apply to being either the radar transmitter or receivers used in this demonstration.

Table 1
Observation Log

Target	Date	Day of year (DOY)	Δt (UTC)	RA (deg)	DEC (deg)	Distance (AU)	POS motion (deg)	P_{TX} (kW)	Receiving antenna
2005 UL5	19 November 2015	323	18:00–22:00	155.7	−09.4	0.016	6	75	Parkes
	21 November 2015	326	01:15–05:05	204.6	−11.6	0.018	7	75	Parkes, ATCA(1.5A)
1998 WT24	9 December 2015	343	11:00–14:55	78.3	+00.2	0.030	2	75	Parkes
	10 December 2015	344	12:00–15:20	68.4	+01.8	0.028	1.3	75	Parkes, ATCA(750C)

Note. Both right ascension (RA) and declination (DEC) are specified for the middle of the observing interval and are in the J2000 epoch; the distance is also specified for the middle of the observing interval; the plane-of-sky (POS) motion is determined from the start of the track to the end; and the transmitter power (P_{TX}) is the average value during the transmissions.

As the radar transmitter, we used the S-band transmitter on DSS-43, the largest steerable antenna in the Southern Hemisphere. Deep Space Network Document 810-005 (2015) provides a comprehensive description of the capabilities of DSS-43; we summarize here key characteristics for this radar demonstration. The S-band transmitter is used routinely for commanding and ranging to spacecraft and operates between 2110 MHz and 2118 MHz, in the spectral allocation for spacecraft uplinks, with a theoretical maximum of 400 kW of transmit power in either circular polarizations (right-circular polarization (RCP) or left-circular polarization (LCP)). The resulting antenna gain is 63 dBi. The transmitted power in this activity was approximately 75 kW, which is 7.3 dB lower than the 400 kW maximum possible power due to derating of the transmitter, which is mission critical to other programs. Furthermore, powers greater than 100 kW will require additional aircraft safety negotiations. Further, system health considerations led us to restrict the transmitted signal to be a simple continuous wave mode, in contrast to the more complicated signal modulations that are possible at the Goldstone Solar System Radar, which can also transmit 500 kW (GSSR, Slade et al., 2011). The typical pointing accuracy at S-band is 4 millidegrees (14.4″), which was found to be adequate for both targets; for reference, the half power beam width at this frequency is 128 millidegrees. At the time of the observations, the uncertainty in the predicted plane-of-sky position of 2005 UL5 was 5.7″ (3σ, JPL orbit solution #40), while that of 1998 WT24 was 1″ (3σ, JPL orbit solution #125). These pointing uncertainties were derived from the statistical orbit solution's measurement covariance matrices mapped to the time and location of the observations.

Using the asteroids' predicted trajectory, the DSS-43 transmitter frequency was continuously adjusted such that the received echo frequency at Parkes would arrive at a constant nominal reference value, essentially compensating on signal uplink for the predicted Doppler frequency shift caused by the asteroid's motion relative to the transmitter and receiver sites. Due to the separation between Parkes and the ATCA on the rotating surface of the Earth, it was not possible to compensate the transmitter frequency for both receivers simultaneously since they experience different frequency shifts. The choice to compensate for Parkes was because it has a higher effective collecting area and, for a first attempt, the focus was on demonstrating the capability.

The receiving antenna used for all of the observations was the 64 m diameter Parkes telescope. These observations made use of one of two wideband feed horns originally built to support Project Phoenix, and the standard (cryogenically cooled) 13 cm receiver (dubbed "Galileo," as it was built to support the tracking of the *Galileo* spacecraft). This receiver-feed horn combination has a nominal bandwidth of 2200 MHz to 2500 MHz but has useful sensitivity as low as 2000 MHz. The slight decrease in sensitivity below 2200 MHz was judged less important than uncertainties in the radar albedos of the targets in planning this demonstration. The system equivalent flux density (SEFD) at the receiver frequency of 2114 MHz was measured as 38 jansky (Jy, 10^{-26} W m^{-2} Hz^{-1}) in each of two circularly polarized outputs, and the beamsize (full width half power) is 10.2′.

The Parkes telescope's standard signal transport system was used to transport the receiver outputs to the control room located in the telescope tower and to provide suitable down-converted outputs for the three recording devices used. All timing and frequency systems within the telescope are locked to an Smithsonian Astrophysical Observatory Hydrogen maser frequency standard. A single polarization (LCP) down converted to 325 MHz was recorded with the Portable Radio Science Recorder (PRSR, Rogstad et al., 2009), provided by Canberra Deep Space Communications Center (CDSCC) for these observations. Additionally, the Observatory's
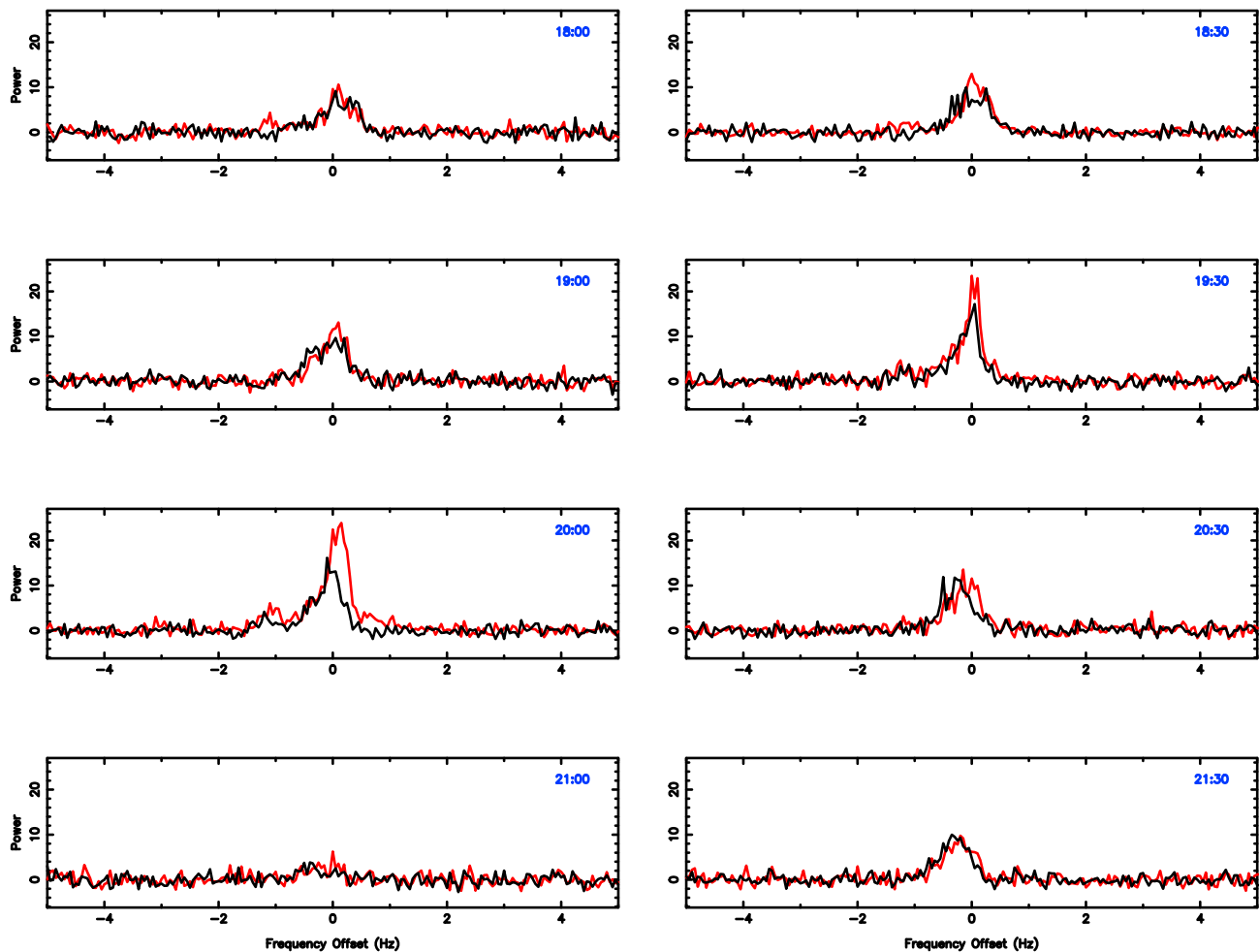
Figure 1. Radar profiles of 2005 UL5 obtained by the DSS-43-Parkes system on 19 November 2015 (DOY 323), for the opposite sense of polarization (OC). Each panel shows the profile averaged over 30 min; the PRSR recorder as analyzed at JPL is shown in black, and the 8 bit VLBI recorder as analyzed by UNSW Australia and the DST Group is shown in red. For all panels, the received echo frequency, relative to the predicted echo frequency, is shown on the abscissa, and the (relative) radar echo power is shown on the ordinate. The frequency resolution is 0.05 Hz, and the radar echo powers are shown in units of the standard deviation of the noise power in the return spectra. There is a clear echo, the shape of which changes over the track, and there is general agreement between the two profiles, from the independent analyses. Not shown are the 2 bit VLBI profiles as they are substantially inferior in quality, due to the lower bit depth and difficulties in excising RFI.

standard very long baseline interferometer (VLBI) recording system (Phillips et al., 2009) was used to record a 4 MHz bandwidth in dual polarization with two Long Baseline Array Data Recorders (LBADRs). One recorder was configured for 2 bit sampling in the standard manner used for VLBI observations (Edwards & Phillips, 2015), while the other was a new configuration for 8 bit sampling, intended to more closely match the PRSR. Data being recorded by both VLBI recorders were monitored in real time.

Following amplification, frequency filtering, and down conversion, the received signals were stored as 8 Msps real signals, with a nominal passband of 0 MHz to 4 MHz. The frequency filtering and offsets were designed to place the expected return in the middle of this passband (i.e., centered at 2 MHz).

One of the goals of these tests was to determine whether the existing VLBI baseband recording system offered a useful adjunct or alternative to the PRSR. In particular, the PRSR is often used in conjunction with spacecraft missions, meaning that any future observations using it would have to be coordinated with other missions. By contrast, the LBA recording system at Parkes is standard and would be much easier to schedule. Further, although the reflected asteroid signal was expected to be predominantly LCP (for an RCP transmitted signal), the dual-polarization capability of VLBI recorders offers the potential of capturing additional information about the characteristics of the reflecting surface.
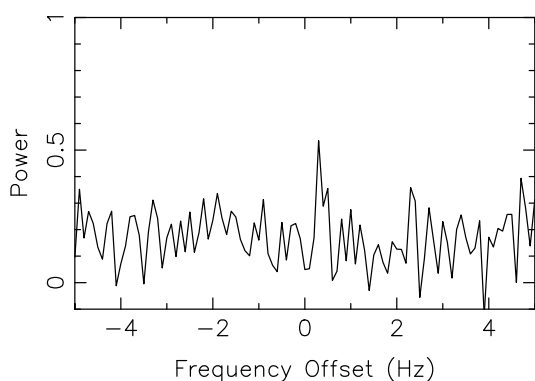
Figure 2. Averaged signal power of 2005 UL5 by the DSS-43-Parkes system on 21 November 2015 (DOY 326). The format is similar to Figure 1, but a return echo was detected only with the PRSR recorder and has been averaged over the entire observation to improve clarity. The vertical scale is an average of the standard deviations. The absence of a detection with the VLBI recorder is likely due to a change in its configuration between the two days.

The Australia Telescope Compact Array (ATCA) is located on CSIRO's Paul Wild Observatory, between the towns of Narrabri and Wee Waa in New South Wales. It is an interferometer consisting of six 22 m diameter, fully steerable parabolic antennas with Cassegrain optics. Five of these antennas can be moved along a 3000 m east-west track and a 214 m north-south track that connects to the east-west track. The configuration of the antennas is changed roughly once every 3 weeks. For the observations on 22 November, the ATCA was in its 1.5A configuration for which the maximum separation among the five track antennas was 1469 m. For the observations on 10 December, it was in its 750C configuration, and the maximum separation between the five track antennas was 750 m. For both sets of observations (and likely any future observations), the inner five antennas were phased together, adding coherently the signals from each, to improve sensitivity; the sixth antenna was sufficiently distant that the phase stability did not allow it to be used. The combined collecting of the five antennas is equivalent to a single antenna with an approximate diameter of 49 m.

The NEA observations used the cryogenically cooled 16 cm receiver, which covers the frequency range 1.1 GHz–3.1 GHz. Each antenna has a system equivalent flux density (SEFD) of 324 Jy in each of the two linearly polarized outputs, but when the outputs from five antennas are combined, this sensitivity improves to 65 Jy. When combined, the signals are also converted from linearly polarized to circularly polarized. The beamsize (full width half power) is 22.2′ per antenna, at the frequency of 2114 MHz used in these observations. When the array is combined, this beamsize is determined by the maximum extent of the array. For the observations of 2005 UL5, the beamsize was approximately $20'' \times 23'$, with the position angle rotating as the observations proceeded; for the observations of 1998 WT24, the beamsize was approximately $40'' \times 23'$, with the position angle also rotating during the course of the observations.

3. Results

Processing of both the PRSR and VLBI format data from Parkes proceeded in a similar manner. For both polarizations, the baseband data were transformed to the frequency domain, using a coherent processing interval sufficient to provide resolution across the expected echo bandwidth. Different frequency resolutions were assessed, and, for many of the results presented, a coherent processing interval of 20 s was used, from which a frequency resolution of 0.05 Hz was obtained.

The noise floor in the received signal varied during the observations, probably as a receiver response to strong radio frequency interference (RFI) that was within the receiver bandwidth but well separated from the asteroid return. The noise floor and received signal amplitude varied in unison by up to 10 dB over the course of an 8 h observation. As a result, the amplitudes of the spectra were normalized by the mean noise level, determined well outside the expected band over which asteroid echoes might be occurring. Further, a small amount of data was excised to account for RFI. The RFI manifested itself as significant changes in the shape of the echo or by the presence of a strong signal at 0 Hz and was particularly noticeable in the Parkes data around a time of 20:00 on 19 November 2015 (DOY 323). These RFI-affected data were excised and not used subsequently for the results presented here.

The individual spectra were then accumulated noncoherently over a sufficient duration to detect the echo from the asteroid. We found that a reasonable integration time was 30 min, sufficient to build up enough signal-to-noise ratio to detect the echo but also with sufficient time resolution to observe changes in the profile of the echo. Figures 1 and 2 show the resulting profiles of 2005 UL5 as measured at Parkes for 19 November 2015 (DOY 323) and 21 November 2015 (DOY 326); for 19 November 2015 (DOY 323), where the signal-to-noise ratio is high enough to justify showing time-resolved profiles, while on 21 November 2015 (DOY 326) the profiles are significantly lower signal-to-noise ratio, consistent with a larger distance to the asteroid (0.016 AU versus 0.023 AU). The DOY 326 signal is so weak that we do not claim it as an unambiguous detection.

Table 2
Time-Resolved Doppler Bandwidths and Estimated Sizes for 2005 UL5

Start time	Doppler width (PRSR) (Hz)	Doppler width (VLBI) (Hz)
18:00	1.30	1.20
18:30	1.15	0.90
19:00	1.10	1.00
19:30	1.90	1.20
20:00	1.75	2.15
20:30	1.20	1.05
21:00	0.75	0.70
21:30	1.10	0.90

Note. The rotation of 2005 UL5 is an open question, so we do not convert these Doppler spreads into size estimates.

Clearly apparent in Figure 1 is that the profiles show changes over the course of the track, consistent with the radar cross section changing as the object rotates. The processing of the signals from the PRSR and VLBI recorders was done independently, and, it is also clear that on 19 November 2015 (DOY 323; Figure 1), the profiles obtained by the independent analyses show good agreement although the strong return between 20:00 and 20:30 may be augmented by RF interference and should be treated with caution. Unfortunately, no echo is detected in the VLBI recorder on 21 November 2015 (DOY 326), likely due to a configuration change in this recorder between the two observations.

We integrated the profiles to obtain the disk-averaged radar cross section σ, following the approach of Benner et al. (1999). We find an approximate value of 9×10^{-3} km^2. By comparison, J. Richardson (private communication, 2015) reports a value of 3.85×10^{-3} km^2 from observations at Arecibo conducted 2 days earlier. Uncertainties on σ can approach 50% due to various calibration uncertainties, and we therefore regard the difference between the two estimates as not significant.

We make measurements of the Doppler width of the asteroid to place crude constraints on its size at such time as a consensus is reached on the rotation rate and axes. Table 2 characterizes the asteroid's size by the Doppler width, determined by the band over which the return exceeds two standard deviations.

The contemporaneous delay-Doppler images obtained by the Goldstone Solar System Radar reveal an object with a long axis of about 300 m and an elongation of about 1.5. The Doppler width values determined by the DSS-43-Parkes system are in good agreement, particularly given the lower signal-to-noise ratios. Further, bandwidth variations of several tens of percent are reasonable given that the interval spanned by the observations covers about 4 h, comparable to the possible rotation period of the asteroid.
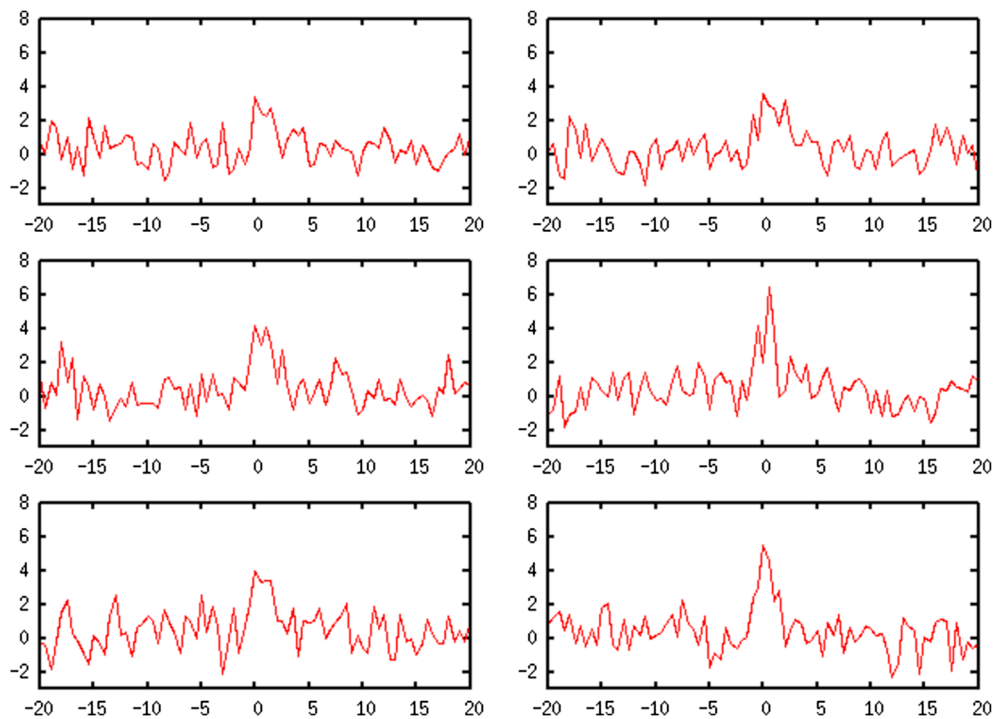

Figure 3. Radar profile for 2 s coherent integration in 30 min blocks starting at 1055 UTC top right through to 1325 UTC at bottom right, from the DSS-43-Parkes observation on 9 December 2015 (DOY 343), in a format similar to Figure 1. Vertical axis is standard deviations; horizontal axis is hertz. Small data segments affected by RFI have been excised.

Figure 3 shows the detection of 1998 WT24 at Parkes. Although the signal-to-noise ratio is poor, the accumulated signal strength is 2–5 standard deviations over each 30 min window, and a noncoherent addition across the entire observation is even stronger.

Finally, neither object was detected in the data recorded at the ATCA. The ATCA is somewhat less sensitive than Parkes, and we attribute the nondetections to the signals being sufficiently marginal that they were not detected. When combined into a tied array, the five 22 m diameter ATCA antennas are equivalent to an approximately 49 m aperture, resulting in the ATCA being only approximately 60% as sensitive as Parkes. Further, the phasing itself is likely to introduce small additional sensitivity losses (~10%). For these observations, the uplink signal was Doppler shifted so that the return frequency at Parkes was effectively constant. Being at a slightly different location, the signal did drift slightly through the receiving band pass, potentially introducing additional small losses. Finally, the predictions for the ATCA tracking positions were computed in a different manner than those for Parkes, which may have led to a pointing offset and additional losses. This combination of reduced sensitivity and additional small processing losses is the likely explanation for the nondetection by the ATCA. Furthermore, prior to the observations, a "Moon bounce" experiment was conducted to calibrate Parkes. The ATCA was not available to participate in this calibration, which could have shown whether an unrecognized aspect of the ATCA configuration is responsible for our lack of a detection. Future asteroid radar attempts using ATCA will include a scheduled Moon bounce to confirm correct operation of the receiving system.

4. Conclusions

We have demonstrated that the detection and study of near-Earth asteroids from the Southern Hemisphere is feasible. Using a bistatic radar approach, we transmitted from Deep Space Station 43 (DSS-43) at the Canberra Deep Space Communications Complex and received with the Parkes Radio Telescope. We detected echoes from both 2005 UL5 and 1998 WT24, the latter being notable because it approached from the south, thereby exemplifying the benefits of having a Southern Hemisphere capability.

There are a number of possible approaches to extending our initial demonstration. First, in principle, the DSS-43 transmitter can transmit with a maximum power of 400 kW. Transmitting at higher powers than we did in this initial demonstration would require consideration of the health of the DSS-43 S-band transmitter and the impact of any transmitter failure on other science missions, as well as radiation clearance to coordinate with any nearby aircraft as approach flight paths to the Canberra Airport can pass close to the CDSCC.

Naidu et al. (2016) have considered the relative performance of various radar systems (both monostatic and bistatic). Among the systems that they considered was the one that we demonstrated here, DSS-43-Parkes. They showed that for the year 2015, nearly 50 NEAs were in principle detectable by this system. While some of these would have also been detectable by one or more of the Northern Hemisphere radar systems, their analysis illustrates that a Southern Hemisphere capability could increase the number of objects tracked. Notably, in 2017, (3122) Florence, which is both one of the largest NEAs and a PHA, will approach from the south, reaching as close as 0.05 AU to the Earth. Perhaps fittingly, (3122) Florence was discovered at the Siding Spring (Australia) during the U.K. Schmidt-Caltech Asteroid Survey.

In addition to DSS-43, there are now three 34 m diameter antennas at CDSCC, equipped with transmitters that operate at 7.1 GHz.(This frequency is in the spectral allocation for Earth-space communications and, in DSN parlance, is termed "X-band" because the corresponding space-Earth communications allocation is in the X-band, though in more general use it would be called "C-band.") One of these 34 m antennas may provide an additional capability, beyond that of DSS-43. The standard DSN 34 m antenna is equipped with a 20 kW X-band transmitter. If one of these antennas were to be used as the transmitter, the ATCA would have to be the receiving system, as Parkes does not have a receiver that covers this frequency. We estimate that this DSN 34 m-ATCA combination, for a 20 kW transmitter, would have a sensitivity approximately a factor of 4 less than the DSS-43-Parkes (S-band) system. Further, this discussion also assumes that the ATCA recording system can be used for radar reception, but, given that the ATCA is routinely used for VLBI observations, we are confident that future investigations will understand and remedy the difficulties encountered here. Moreover, long-term DSN planning is for at least one CDSCC 34 m antenna to be equipped with an 80 kW transmitter. If realized, an 80 kW, X-band system would be comparable to the system demonstrated here, unless and until the DSS-43 transmitter power can be increased above 100 kW.

References

Benner, L. A. M., Hudson, R. S., Ostro, S. J., Rosema, K. D., Giorgini, J. D., Yeomans, D. K., … Pravec, P. (1999). Radar observations of asteroid 2063 Bacchus. *Icarus*, *139*, 309–327. https://doi.org/10.1006/icar.1999.6094

Busch, M. W., Benner, L. A. M., Ostro, S. J., Lance A. M., Giorgini, J. D., Jurgens, R. F., … Hine, A. A. (2008). Physical properties of near-Earth asteroid (33342) 1998 WT24. *Icarus*, *195*, 614–621. https://doi.org/10.1016/j.icarus.2008.01.020

Campbell, B. A., Campbell, D. B., Chandler, J. F., Hine, A. A., Nolan, M. C., & Perillat, P. J. (2003). Radar imaging of the lunar poles. *Nature*, *426*, 137–138.

Chesley, S. R., Farnocchia, D., Nolan, M. C., Vokrouhlický, D., Chodas, P. W., Milani, A., … Taylor, P. A. (2014). Orbit and bulk density of the OSIRIS-REx target Asteroid (101955) Bennu. *Icarus*, *235*, 5–22. https://doi.org/10.1016/j.icarus.2014.02.020

Committee to Review Near-Earth-Object Surveys (2010). *Defending Planet Earth: Near-Earth-Object Surveys and Hazard Mitigation Strategies*. Washington, DC: National Academies Press.

Deep Space Network Document 810-005 (2015). *70-m Subnet Telecommunications Interfaces, Rev. F*, August 5, Jet Propulsion Laboratory, California Institute of Technology, Pasadena, CA. http://deepspace.jpl.nasa.gov/dsndocs/810-005/

Di Martino, M., Montebugnoli, S., Cevolani, G., Ostro, S., Zaitsev, A., Righini, S., … Gavrik, Y. (2004). Results of the first Italian planetary radar experiment. *Planetary and Space Science*, *52*, 325–330. https://doi.org/10.1016/j.pss.2003.09.001

Edwards, P. G., & Phillips, C. (2015). The long baseline array. *Publications of The Korean Astronomical Society*, *30*, 659–661.

Giorgini, J. D., Benner, L. A. M., Brozovic, M., Busch, M. W., Campbell, D. B., Chesley, S. R., … Yeomans, D. K. (2009). Radar astrometry of small bodies: Detection, characterization, trajectory prediction, and hazard assessment, White Paper, submitted to the Planetary Sciences Decadal Survey (2013–2022). https://trs.jpl.nasa.gov/handle/2014/45703

Giorgini, J. D., Chodas, P. W., Slade, M. A., Preston, R. A., & Yeomans, D. K. (2008). DSN radar upgrade study, Jet Propulsion Laboratory, National Aeronautics and Space Administration, Pasadena, CA. http://hdl.handle.net/2014/45704

Giorgini, J. D., Slade, M. A., Silva, A., Preston, R. A., Brozovic, M., Taylor, P. A., & Magri, C. (2009). Improved impact hazard assessment with existing radar sites and a new 70-M Southern Hemisphere radar installation, Jet Propulsion Laboratory, National Aeronautics and Space Administration, Pasadena, CA. http://hdl.handle.net/2014/45220

Harmon, J. K., Slade, M. A., Vélez, R. A., Crespo, A., Dryer, M. J., & Johnson, J. M. (1994). Radar mapping of Mercury's polar anomalies. *Nature*, *369*, 213–215. https://doi.org/10.1038/369213a0

Muhleman, D. O., Butler, B. J., Grossman, A. W., & Slade, M. A. (1991). Radar images of Mars. *Science*, *253*, 1508–13. https://doi.org/10.1126/science.253.5027.1508

Muhleman, D. O., Grossman, A. W., Butler, B. J., & Slade, M. A. (1990). Radar reflectivity of Titan. *Science*, *248*, 975–80. https://doi.org/10.1126/science.248.4958.975

Naidu, S. P., Benner, L. A. M., Margot, J.-L., Busch, M. W., & Taylor, P. A. (2016). Capabilities of Earth-based radar facilities for near-Earth asteroid observations. *Astronomical Journal*, *152*, 99.

Ostro, S. J. (2007). Planetary radar. In McFadden, L. A., Weissman, P. R., & Johnson, T. V. (Eds.), *Encyclopedia of the Solar System* (2nd ed., pp. 735–764): Academic Press.

Ostro, S. J., & Giorgini, J. D. (2004). The role of radar in predicting and preventing asteroid and comet collisions with Earth, *Mitigation of Hazardous Comets and Asteroids* (38 pp.). Cambridge: Cambridge University Press.

Ostro, S. J., & Pettengill, G. H. (1978). Icy craters on the Galilean satellites. *Icarus*, *34*, 268–279. https://doi.org/10.1016/0019-1035(78)90167-7

Phillips, C., Tzioumis, T., Tingay, S., Stevens, J., Lovell, J., Amy, S., … Dodson, R. (2009). LBADR: The LBA data recorder. In *Science and Technology of Long Baseline Real-Time Interferometry : 8th International e-VLBI Workshop - EXPReS09*, Madrid, Spain, 99 pp.

Rogstad, S., Navarro, R., Finley, S., Goodhart, C., Proctor, R., & Asmar, S. (2009). Portable Radio Science Receiver (RSR) (*Interplanetary Network Progress Report, 178, 1*), Jet Propulsion Laboratory, California Institute of Technology, Pasadena, CA. http://adsabs.harvard.edu/abs/2009IPNPR.178B...1R

Slade, M. A., Benner, L. A. M., & Silva, A. (2011). Goldstone solar system radar observatory: Earth-based planetary mission support and unique science results. *Proceedings of the IEEE*, *99*, 757–769. https://doi.org/10.1109/ JPROC.2010.2081650

Slade, M. A., Butler, B. J., & Muhleman, D. O. (1992). Mercury radar imaging—Evidence for polar ice. *Science*, *258*, 635–640. https://doi.org/10.1126/science.258.5082.635

Stacy, N. J. S., Campbell, D. B., & Ford, P. G. (1997). Arecibo radar mapping of the lunar poles: A search for ice deposits. *Science*, *276*, 1527–1530. https://doi.org/10.1126/science.276.5318.1527